Springer

KSME

Journal of Mechanical Science and Technology 29 (7) (2015) 3017~3029
www.springerlink.com/content/1738-494x(Print)/1976-3824(Online)
DOI 10.1007/s12206-015-0632-x

Thermodynamic performance analysis of a coupled transcritical and subcritical organic Rankine cycle system for waste heat recovery †

Xi-Wu Gong[1], Xiao-Qiong Wang[2], You-Rong Li[2,*] and Chun-Mei Wu[2]

[1]*School of Naval Architecture and Ocean Engineering, Zhejiang Ocean University, Zhejian 316022, China*
[2]*Key Laboratory of Low-grade Energy Utilization Technologies and Systems of Ministry of Education, College of Power Engineering, Chongqing University, Chongqing 400044, China*

(Manuscript Received November 24, 2014; Revised March 8, 2015; Accepted March 22, 2015)

Abstract

We present a novel coupled organic Rankine cycle (CORC) system driven by the low-grade waste heat, which couples a transcritical organic Rankine cycle with a subcritical organic Rankine cycle. Based on classical thermodynamic theory, a detailed performance analysis on the novel CORC system was performed. The results show that the pressure ratio of the expander is decreased in the CORC and the selection of the working fluids becomes more flexible and abundant. With the increase of the pinch point temperature difference of the internal heat exchanger, the net power output and thermal efficiency of the CORC all decrease. With the increase of the critical temperature of the working fluid, the system performance of the CORC is improved. The net power output and thermal efficiency of the CORC with isentropic working fluids are higher than those with dry working fluids.

Keywords: Coupled organic Rankine cycle; Thermodynamic analysis; Waste heat recovery; Working fluid combination

1. Introduction

The organic Rankine cycle (ORC) is an effective way to convert waste heat into power. It has many advantages, such as simple construction, flexibility, safety, low operation cost and high recovery efficiency [1, 2]. In the ORC, an organic fluid with the low boiling point temperature is used as the working fluid, which is different from the steam Rankine cycle. Up to now, many investigations on the ORC have been made to improve the system performance, including parameter optimization, working fluid selection and economic evaluation etc. [3-6].

In a subcritical organic Rankine cycle (SORC) the irreversible loss in the evaporator is an important factor that influences the system efficiency [7, 8]. To decrease the irreversibility in the evaporator, a transcritical organic Rankine cycle (TORC) has been proposed [9-11]. The TORC can improve the system performance by adjusting the temperature match between the heat source and the working fluid. Algieri et al. [12] did a comparative energetic analysis on the SORC and TORC systems and found that the thermal efficiency of the TORC is higher than that of the SORC under the same heat source and heat sink conditions. Zhang et al. [13] examined the thermodynamic and economic performance of both the SORC and TORC systems for the low-temperature geothermal power plant. The results showed that the TORC with R125 as the working fluid is a cost effective approach for the low-temperature geothermal ORC system. It yields a high recovery efficiency and relatively low cost. Mikielewicz et al. [14] introduced a thermodynamic criterion to select the suitable working fluid for the SORC and TORC systems, and the theoretical performance of the ORC with twenty working fluids was assessed. The TORC system exhibited higher efficiency than the SORC system, and the improvement was about 5% in the overall efficiency referred to the SORC system.

Although the TORC has potential to improve the thermal efficiency owing to a good thermal match in the evaporator, the highest pressure and pressure ratio in the expander are generally larger than those in the SORC [14, 15]. In a small ORC, the single screw expander is widely used due to the simple construction, high efficiency, and tolerable two-phase [16, 17]. However, the permissive pressure ratio in the single screw expander is low [18-20]. For example, it is limited to 8 in the works of Wang et al. [21, 22]. The limitation of the pressure ratio results in a small pressure variation in the expander and an increase of the condensing temperature of the working fluid in the condenser [12, 15]. Therefore, there is a decrease possibility of the thermal efficiency in the TORC

*Corresponding author. Tel.: +86 23 65112284, Fax.: +86 23 65102473
E-mail address: liyourong@cqu.edu.cn
† Recommended by Associate Editor Tong Seop Kim

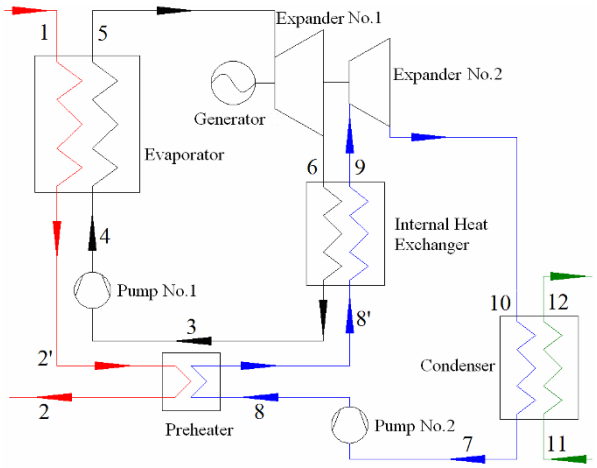

Fig. 1. Schematic diagram of the configuration.

system. As a consequence, a two-stage cycle was introduced by some researchers. Wang et al. [23] proposed a novel two-stage cycle which combined a dual loop ORC with a gasoline engine. The results proved that the net power output and thermal efficiency are all increased. Meinel et al. [24] presented another two-stage ORC concept and carried on the performance comparison of the standard ORC and the two-stage cycle. However, the same working fluid is used in the two subsystems for these two-stage cycles. Xu et al. [25] studied the effect of the critical temperature of the working fluids on the thermal performance of the TORC system in three operating models and found that the working fluid with the high critical temperature yields a small integrated-average temperature difference and the high system exergy efficiency. Therefore, the working fluid adapted to different temperature region should be different in the two-stage cycle.

To solve the above problems, we introduced a novel coupled organic Rankine cycle (CORC) system driven by the waste heat of the flue gas that is released from industrial boilers, which couples a transcritical organic Rankine cycle with a subcritical organic Rankine cycle. In this work, thermodynamic analysis of the CORC system performance was performed by Refprop 8.0 [26]. A performance comparison between the TORC and the CORC was also presented.

2. System configuration descriptions

The novel coupled organic Rankine cycle system consists of a TORC and a SORC, as shown in Fig. 1. The internal heat exchanger plays two different roles in the CORC system: a condenser for the TORC subsystem and a vapor generator for the SORC subsystem. The exhaust vapor from the TORC subsystem is cooled and condensed by the working fluid of the SORC subsystem in the internal heat exchanger. At the same time, the working fluid of the SORC subsystem absorbs heat and turns into saturated vapor.

In the CORC, the single screw expander is used. Because of two-stage expansion, the pressure ratio in every expander is reduced. Therefore, the expander can operate at the optimal pressure ratio range to keep higher isentropic expansion efficiency. Furthermore, a preheater is equipped to improve the recovery efficiency of the waste heat of the flue gas and increase the net power output of the CORC. Meanwhile, the different working fluids are selected for the TORC and the SORC subsystems. Compared with the traditional TORC, the novel CORC avoids the limitation of the pressure ratio and increases the power output of the single screw expander. In the TORC and SORC subsystems, all the temperature variation ranges of the heat sources are reduced. Therefore, the selection of the working fluids becomes more flexible and abundant, which provides a possibility to improve the thermal efficiency of the CORC.

As we know, the working fluid has an important influence on the ORC system performance. In the CORC system, two different working fluids are, respectively, applied in the TORC and the SORC subsystems. The selections of the working fluids are restricted by the critical parameter of the fluids, as well as the heat source and sink conditions. At the same time, thermodynamic performance, safety, viscosity, flammability, stability and environmental impact of the working fluids also need to be considered [27]. In this work, eighteen kinds of the working fluids with different critical temperatures are selected for the CORC system to obtain the optimal combination of the working fluids after comprehensive consideration. Thermo-physical properties of the selected working fluids and the critical parameters are presented in Table 1.

Table 1. Thermo-physical properties and the critical parameters of the working fluids.

Working fluids	M kg/kmol	T_{cri} °C	P_{cri} MPa	ρ_{cri} kg/m^3	Fluid type
RC318	200.04	115.23	2.778	569.15	Dry
R124	136.48	122.28	3.624	539.07	Isentropic
R236fa	152.04	124.92	3.20	551.04	Dry
Isobutane	58.12	134.66	3.629	224.59	Isentropic
R236ea	152.04	139.29	3.502	833.70	Dry
R114	170.92	145.68	3.257	720.36	Dry
R600	58.12	151.98	3.796	227.35	Isentropic
R245fa	134.05	154.01	3.651	489.31	Isentropic
Neopentane	72.15	160.59	3.196	214.96	Dry
Cis-butene	56.11	162.6	4.226	191.10	Isentropic
R245ca	134.05	174.42	3.925	516.14	Dry
R123	152.93	183.68	3.662	524.99	Isentropic
Isopentane	72.15	187.2	3.378	215.65	Dry
N-pentane	72.15	196.55	3.37	207.74	Dry
R141b	116.95	204.35	4.212	492.97	Isentropic
R113	187.38	214.06	3.392	530.16	Dry
Isohexane	86.18	224.55	3.04	203.38	Dry
N-hexane	86.18	234.67	3.034	183.50	Dry

Table 2. Main parameters and boundary conditions of the CORC.

Parameters	Values	Refs.
Ambient temperature, T_0 (°C)	20	[25, 33]
Mass flow rate of flue gas, m_g (kg/s)	10	[4]
Inlet temperature of flue gas, T_1 (°C)	240-400	
Outlet temperature of flue gas, T_2 (°C)	80-120	
Inlet temperature of cooling water, T_{11} (°C)	20	[25, 33]
Outlet temperature of cooling water, T_{12} (°C)	25	[25]
Condensation temperature, T_7 (°C)	30	[25, 32]
Expander isentropic efficiency, η_{exp}	0.8	[30, 32, 34]
Working pump isentropic efficiency, η_p	0.7	[30, 32, 34]
Pressure ratio of the expander, ε_p	2-8	[21-22]

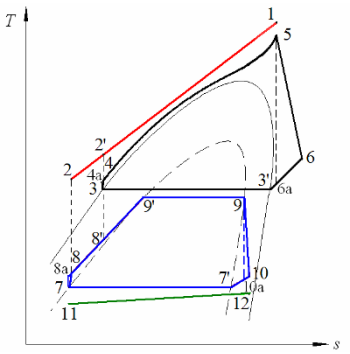

Fig. 2. The *T-s* diagram of the CORC system.

3. Mathematical model

The *T-s* diagram of the CORC is shown in Fig. 2. To simplify the calculation, the following assumptions are considered [28-30]:

(1) All components are operated under the steady state;

(2) The heat loss and pressure loss in the heat exchangers and pipelines are small enough to be neglected;

(3) The working fluids at the outlet of the internal heat exchanger and the condenser are saturated states (saturated liquid or vapor);

(4) The highest temperature of the working fluid in the TORC subsystem is assigned to be 20°C below the flue gas inlet temperature [31, 32].

For the effective operation of the evaporator in the TORC subsystem, the minimum pinch point temperature difference (PPTD) in the evaporator is not less than 5°C. To avoid low temperature corrosion, the lowest outlet temperature of the flue gas should be above 80°C. The composition of the selected flue gas is carbon dioxide, vapor and nitrogen gas, and the corresponding mass fractions are 13%, 11% and 76%, respectively. In the performance analysis of the CORC, a set of main parameters and boundary conditions of the flue gas and cooling water, and some cycle parameters are set, as shown in Table 2.

On the basis of the first and second law of thermodynamics, the mathematical model of the CORC can be described as follows.

For the TORC subsystem, the heat and mass flow rate of the working fluid in the evaporator can be expressed as:

$$Q_e = m_g(c_{p,g1}T_1 - c_{p,g2'}T_{2'}) \quad (1)$$

$$m_{wf1} = Q_e / (h_5 - h_4) = m_g(c_{p,g1}T_1 - c_{p,g2'}T_{2'}) / (h_5 - h_4) \quad (2)$$

where, T_1 and $T_{2'}$ are the inlet and outlet temperatures of the flue gas in the evaporator, $c_{p,g1}$ and $c_{p,g2'}$ are the corresponding specific heat capacities of the flue gas, h_4 and h_5 are the enthalpies of the working fluid at the inlet and outlet of the evaporator, respectively.

The output power of the expander No.1 and the power consumption of the pump No.1 can be calculated by the following equations:

$$W_{exp1} = m_{wf1}(h_5 - h_6) = m_{wf1}\eta_{exp}(h_5 - h_{6,a}), \quad (3)$$

$$W_{p1} = m_{wf1}(h_4 - h_3) = m_{wf1}(h_{4,a} - h_3) / \eta_p, \quad (4)$$

where, h_3 is the enthalpy of the working fluid at the inlet of the pump No.1, $h_{6,a}$ and $h_{4,a}$ are the enthalpies of the working fluid at the outlet of the expander No.1 and the pump No.1 under the isentropic expansion and compression conditions, respectively. η_{exp} and η_p are the isentropic efficiencies of the expander No.1 and the pump No.1, which are defined as, respectively

$$\eta_{exp} = (h_5 - h_6) / (h_5 - h_{6,a}), \quad (5)$$

$$\eta_p = (h_{4,a} - h_3) / (h_4 - h_3). \quad (6)$$

For the SORC subsystem, the heat and mass flow rate of the working fluid in the internal heat exchanger are, respectively,

$$Q_{ihe} = m_{wf1}(h_6 - h_3) = m_{wf2}(h_9 - h_{8'}), \quad (7)$$

$$m_{wf2} = Q_{ihe} / (h_9 - h_{8'}) = m_{wf1}(h_6 - h_3) / (h_9 - h_{8'}), \quad (8)$$

where, $h_{8'}$ and h_9 are the enthalpies of the working fluid at the inlet and outlet of the internal heat exchanger, respectively.

The output power of the expander No.2 and the power consumption of the pump No.2 can be calculated as following equations, respectively:

$$W_{exp2} = m_{wf2}(h_9 - h_{10}) = m_{wf2}\eta_{exp}(h_9 - h_{10,a}), \quad (9)$$

$$W_{p2} = m_{wf2}(h_8 - h_7) = m_{wf2}(h_{8,a} - h_7) / \eta_p, \quad (10)$$

where, h_7 and h_8 are the enthalpies of the working fluid at the inlet and outlet of the pump No.2, respectively. h_{10} is the enthalpy of the working fluid at the outlet of the expander No.2, $h_{10,a}$ and $h_{8,a}$ are the enthalpies of the working fluid at the outlet of the expander No.2 and the pump No.2 under the isen-

tropic expansion and compression conditions, respectively. η_{exp} and η_p are the isentropic efficiencies of the expander No.2 and the pump No.2,

$$\eta_{exp} = (h_9 - h_{10}) / (h_9 - h_{10,a}) , \quad (11)$$

$$\eta_p = (h_{8,a} - h_7) / (h_8 - h_7) . \quad (12)$$

The heat and mass flow rate of water in the condenser can be expressed as:

$$Q_c = m_w c_{p,w} (T_{12} - T_{11}) = m_{wf2} (h_{10} - h_7) , \quad (13)$$

$$m_w = \frac{Q_c}{c_{p,w}(T_{12} - T_{11})} = \frac{m_{wf2}(h_{10} - h_7)}{c_{p,w}(T_{12} - T_{11})} \quad (14)$$

where, T_{11} and T_{12} are the inlet and outlet temperatures of the cooling water in the condenser, $c_{p,w}$ is the corresponding specific heat capacity of the cooling water.

The heat flow rate in the preheater can be calculated as:

$$Q_{pre} = m_g (c_{p,g2} T_{2'} - c_{p,g2} T_2) = m_{wf2} (h_{8'} - h_8) , \quad (15)$$

where, T_2 is the outlet temperature of the flue gas in the preheater, $c_{p,g2}$ is the corresponding specific heat capacity of the flue gas.

The net power output and thermal efficiency of the CORC can be respectively expressed as

$$W_{net} = (W_{exp1} - W_{p1}) + (W_{exp2} - W_{p2}) , \quad (16)$$

$$\eta_{th} = W_{net} / (Q_e + Q_{pre}) . \quad (17)$$

4. Results and discussion

To understand the effects of the main parameters on the thermodynamic performance of the CORC, R123 and R245fa are respectively selected as the working fluids of the TORC and SORC subsystems in this section. This combination of the working fluids is denoted as "R123/R245fa".

The pressure ratio ε_p of the expander is defined as the inlet pressure divided by the outlet pressure [21, 35]. In this work, the single screw expander is used and the maximum pressure ratio is limited to ε_p = 8. In general, the isentropic expansion efficiency of the single screw expander is dependent on the pressure ratio [36-38]. For simplification, it is fixed at 80% in the CORC due to a small pressure ratio.

The pressure ratio has an important influence on the CORC performance. Fig. 3 shows the variations of the net power output W_{net} and the thermal efficiency η_{th} with the pressure ratio ε_{p1} of the expander No.1 in the TORC subsystem at T_1 = 270°C, T_2 = 90°C, $T_{2'}$ = 120°C, P_5 = 1.03P_{cri1} [12, 39] and ΔT_{ihe} = 5°C [30, 32]. Here, ΔT_{ihe} is the pinch point temperature difference of the internal heat exchanger. There is an optimal pressure ratio corresponding to the maximum net power output. However, the PPTD (ΔT_e) of the evaporator exceeds the limitation condition of 5°C at the maximum net power output, that is ΔT_e < 5°C. Therefore, the maximum net power output satisfying with the limitation condition of the PPTD is obtained at an appropriate value ε_{p1} = 5.04, where ΔT_e = 5°C. Hereafter, this appropriate value of the pressure ratio is called as the optimal pressure ratio. The optimal pressure ratio ε_{p2} of the expander No.2 in the SORC subsystem depends on the pressure ratio ε_{p1}, that is, ε_{p2} = 6.05. As the thermal efficiency is determined by the net power output at the same heat source and heat sink conditions, the thermal efficiency has the same variation with the net power output. In addition, the thermodynamic properties of working fluids at each state point of the CORC are listed in Table 3 at the optimal pressure ratios. In

Table 3. Thermodynamic properties of working fluids at each state point of the CORC at T_1 = 270°C, T_2 = 90°C, $T_{2'}$ = 120°C, P_5 = 1.03P_{cri1}, ε_{p1} = 5.04 and ε_{p2} = 6.05.

State	Fluid	P MPa	T °C	h kJ/kg	s kJ/kg K	m kg/s
1	Flue gas	0.101	270	767.91	6.892	10
2'	Flue gas	0.101	120	602.69	6.537	10
2	Flue gas	0.101	90	570.34	6.451	10
3'	R123	0.748	97.84	438.64	1.685	7.18
3	R123	0.748	97.84	303.30	1.321	7.18
4	R123	3.772	100.84	306.73	1.323	7.18
5	R123	3.772	250	548.06	1.862	7.18
6	R123	0.748	191.08	518.86	1.878	7.18
7'	R245fa	0.178	30	426.43	1.753	8.17
7	R245fa	0.178	30	239.10	1.135	8.17
8	R245fa	1.075	30.54	240.07	1.136	8.17
8'	R245fa	1.075	60.66	281.28	1.266	8.17
9'	R245fa	1.075	92.84	328.63	1.401	8.17
9	R245fa	1.075	92.84	469.97	1.787	8.17
10	R245fa	0.178	47.62	443.50	1.808	8.17
11	Water	0.101	20	84.01	0.296	79.85
12	Water	0.101	25	104.92	0.367	79.85

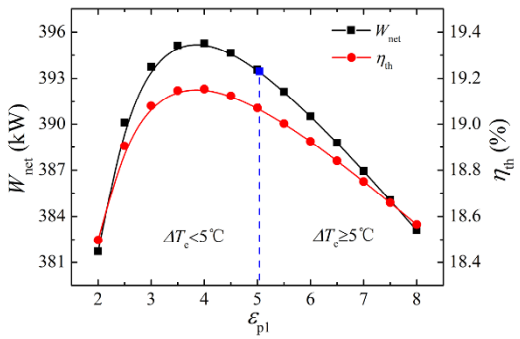

Fig. 3. Variations of net power output W_{net} and thermal efficiency η_{th} with the pressure ratio ε_{p1} at T_1 = 270°C, T_2 = 90°C, $T_{2'}$ = 120°C, P_5 = 1.03P_{cri1} and ΔT_{ihe} = 5°C.

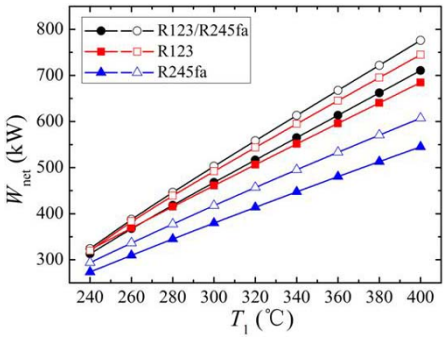

(a)

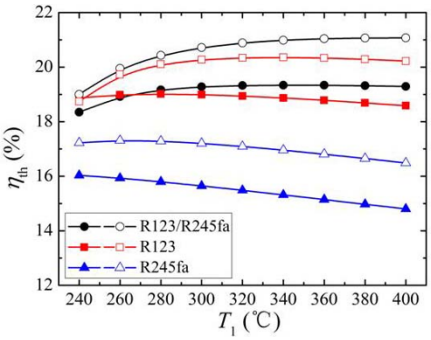

(b)

Fig. 4. Variations of net power output W_{net} (a) and thermal efficiency η_{th}; (b) with inlet temperature of the flue gas T_1 at T_2 = 90°C, $T_{2'}$ = 120°C and ΔT_{ihe} = 5°C. Solid symbols: $P_5 = 1.03P_{cri1}$; hollow symbols: $P_5 = 1.6P_{cri1}$.

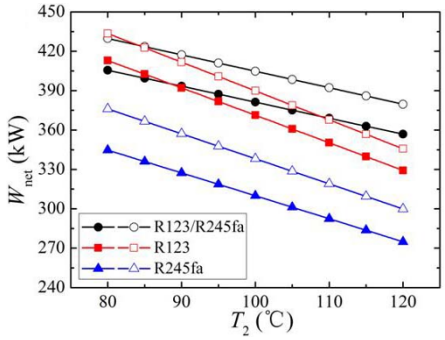

(a)

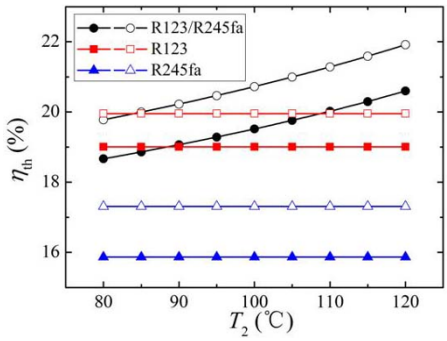

(b)

Fig. 5. Variations of net power output W_{net} (a) and thermal efficiency η_{th}; (b) with outlet temperature T_2 of the flue gas at T_1 = 270°C, $T_{2'}$ = 120°C and ΔT_{ihe} = 5°C. Solid symbols: $P_5 = 1.03P_{cri1}$; hollow symbols: $P_5 = 1.6P_{cri1}$.

this case, the amount of heat exchanged in the internal heat exchanger is 1547.7 kW. In the following results, the pressure ratio is always fixed at the optimal pressure ratios.

4.1 Effect of the flue gas temperature

The temperature of the flue gas is a key parameter that influences the CORC performance. Fig. 4 gives the variations of the net power output W_{net} and thermal efficiency η_{th} of the CORC with the inlet temperature T_1 of the flue gas under two pressure conditions at T_2 = 90°C, $T_{2'}$ = 120°C and ΔT_{ihe} = 5°C. The results of the traditional TORC with R123 and R245fa as the working fluids are also shown in Fig. 4. Obviously, at a high inlet temperature of the flue gas, the heat transfer in the evaporator is enhanced. The mass flow rate and the temperature of the working fluid at the inlet of the expander No.1 are increased. Therefore, the net power output is increased with the increase of the inlet temperature of the flue gas.

At $P_5 = 1.03P_{cri1}$, the traditional R245fa-based TORC shows the lowest net power output. Furthermore, there is a threshold inlet temperature between the CORC and the traditional R123-based TORC. At T_1>265.2°C, the net power output of the CORC is higher than that of the traditional R123-based TORC. However, the result is otherwise at T_1 < 265.2°C. At $P_5 = 1.6P_{cri1}$, the traditional R245fa-based TORC also yields the lowest value. While the net power output of the CORC is always higher than that of the traditional R123-based TORC. Note that there is no limit to the pressure ratio of the expander in the traditional TORCs.

On the other hand, the thermal efficiency is determined by the net power output and the total heat flow rate. With the increase of the inlet temperature of the flue gas, both the net power output and the total heat flow rate increase. However, their variation rates are different, which results in the variation of the thermal efficiency, as shown in Fig. 4(b). As a result, when $P_5 = 1.03P_{cri1}$, the thermal efficiency of the CORC increases, and that of the traditional R123-based TORC has a slight variation, while that of the traditional R245fa-based TORC decreases. When $P_5 = 1.6P_{cri1}$, the thermal efficiencies of the CORC and the traditional R123-based TORC all increase, while that of the traditional R245fa-based TORC decreases.

The effects of the outlet temperature T_2 of the flue gas on the net power output and thermal efficiency are shown in Fig. 5 at T_1 = 270°C, $T_{2'}$ = 120°C and ΔT_{ihe} = 5°C. As expected, the net power output decreases linearly with the increase of the outlet temperature of the flue gas. However, the decrease rate of the net power output of the CORC is always lower than those of the traditional TORCs, and the lowest net power output appears in the traditional R245fa-based TORC, as shown in Fig. 5(a). The increase of the outlet temperature of the flue gas results in the decrease of the total heat flow rate and the

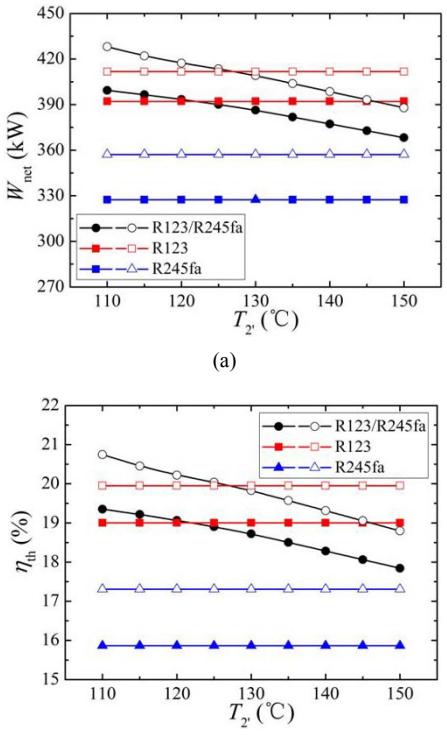

Fig. 6. Variations of net power output W_{net} (a) and thermal efficiency η_{th}; (b) with outlet temperature $T_{2'}$ of the flue gas in the evaporator at T_1 = 270°C, T_2 = 90°C and ΔT_{ihe} = 5°C. Solid symbols: $P_5 = 1.03P_{cri1}$; hollow symbols: $P_5 = 1.6P_{cri1}$.

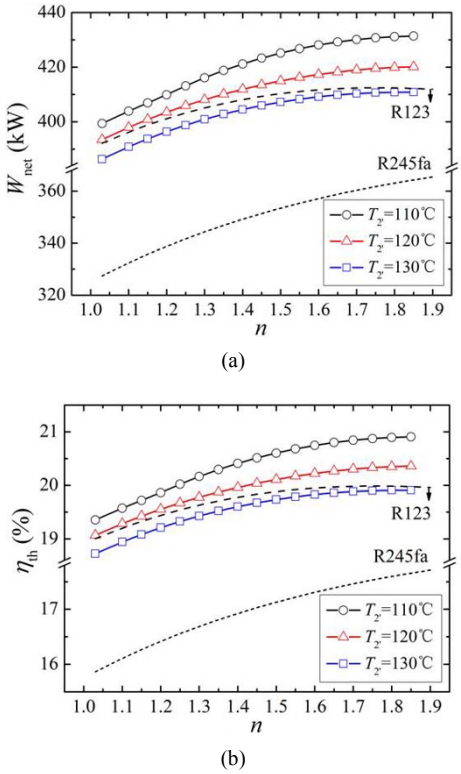

Fig. 7. Variations of net power output W_{net} (a) and thermal efficiency η_{th}; (b) with the inlet pressure P_5 of the expander No.1 at T_1 = 270°C, T_2 = 90°C and ΔT_{ihe} = 5°C. Hollow symbols: R123/R245fa.

net power output. Because the decrease rate of the net power output is lower than that of the total heat flow rate, the thermal efficiency of the CORC increases with the increase of the outlet temperature of the flue gas. However, the thermal efficiency of the traditional TORC is almost independent of the outlet temperature of the flue gas, as shown in Fig. 5(b). At $P_5 = 1.03P_{cri1}$, the threshold outlet temperature of the flue gas is T_2 = 88.5°C, where the CORC and the traditional R123-based TORC have the same net power output and thermal efficiency. When $T_2 > 88.5$°C, the net power output and the thermal efficiency of the CORC are higher than those of the traditional R123-based TORC. At $P_5 = 1.6P_{cri1}$, the threshold outlet temperature of the flue gas is T_2 = 84.0°C.

Fig. 6 shows the variations of the net power output and thermal efficiency with the outlet temperature $T_{2'}$ of the flue gas in the evaporator at T_1 = 270°C, T_2 = 90°C and ΔT_{ihe} = 5°C. In the traditional TORCs, the net power output and thermal efficiency remain constant. However, in the CORC, the net power output of the TORC subsystem with higher thermal efficiency decreases, while that of the SORC subsystem with lower thermal efficiency increases. As a result, the total net power output of the CORC is reduced with the increase of the outlet temperature $T_{2'}$ of the flue gas in the evaporator, as shown in Fig. 6(a). Obviously, the lowest net power output is still produced by the traditional R245fa-based TORC. Correspondingly, the thermal efficiency of the CORC is also reduced, as shown in Fig. 6(b). When $T_{2'} < 121.9$°C, the net power output and the thermal efficiency of the CORC are higher than those of the traditional R123-based TORC at $P_5 = 1.03P_{cri1}$. However, at $P_5 = 1.6P_{cri1}$, this transition outlet temperature of the flue gas in the evaporator is $T_{2'}$ = 127.0°C.

4.2 Effect of the inlet pressure of the expander No.1

To ensure the inlet pressure of the expander No.1 greater than the critical pressure of working fluid in the TORC subsystem and simplify the expression, a coefficient n is introduced. The inlet pressure of the expander No.1 is expressed as $P_5 = n*P_{cri1}$, and thereby, P_{cri1} is the critical pressure of the working fluid of the TORC subsystem and n is a coefficient. It is obvious that n>1. Therefore, the inlet pressure P_5 of the expander No.1 is determined by the coefficient n.

Fig. 7 illustrates the variations of the net power output and thermal efficiency with the inlet pressure P_5 of the expander No.1 at T_1 = 270°C, T_2 = 90°C and ΔT_{ihe} = 5°C. It is found that the inlet pressure of the expander No.1 has a positive effect on the net power output and thermal efficiency of the CORC. In the CORC, the maximum pressure ratio of the expander and the minimum PPTD of the evaporator are limited to 8 and 5°C, respectively. Therefore, the maximum inlet pressure of the expander No.1 is $P_5 = 1.85P_{cri1}$. In this case, the maximum net power output of the CORC is 420.1 kW at $T_{2'}$ =

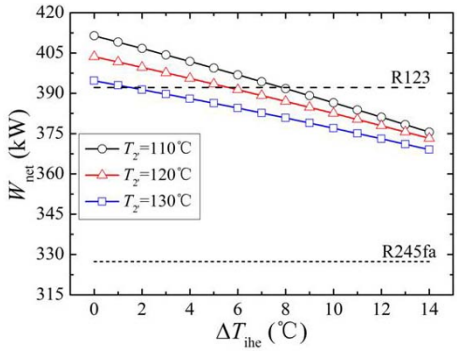

(a)

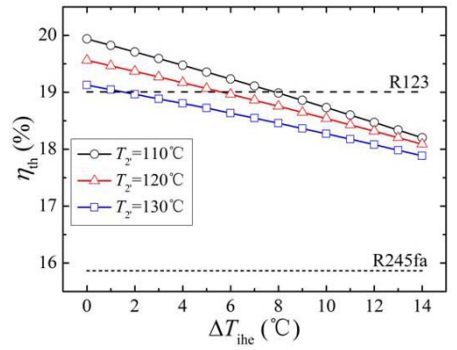

(b)

Fig. 8. Variations of net power output W_{net} (a) and thermal efficiency η_{th}; (b) with the PPTD of the internal heat exchanger at T_1 = 270°C, T_2 = 90°C and $P_5 = 1.03P_{cri1}$. Hollow symbols: R123/R245fa.

120°C. For the traditional TORCs, there is no limitation of the pressure ratio. The inlet pressure of the expander has an optimal value of $P_5 = 1.75P_{cri1}$ corresponding to the maximum net power output for the traditional R123-based TORC, and the maximum net power output is 412.5 kW. Note that the effect of the inlet pressure P_5 of the expander No.1 on the CORC performance increases with the decrease of the outlet temperature of the flue gas in the evaporator. The variation of the thermal efficiency is the same with that of the net power output, as shown in Fig. 7(b).

4.3 Effect of the PPTD of the internal heat exchanger

The internal heat exchanger couples the TORC and SORC subsystems in the CORC. Therefore, the pinch point temperature difference (ΔT_{ihe}) of the internal heat exchanger has an important influence on the CORC performance. Theoretically, the CORC exhibits the best thermodynamic performance at ΔT_{ihe} = 0°C. With the increase of the PPTD of the internal heat exchanger, the net power output and thermal efficiency of the CORC are decreased. Fig. 8 shows the variations of the net power output and thermal efficiency with the PPTD (ΔT_{ihe}) of the internal heat exchanger at T_1 = 270°C, T_2 = 90°C and $P_5 = 1.03P_{cri1}$. It is predicted that the increase of the outlet temperature of the flue gas in the evaporator weakens the effect of the PPTD of the internal heat exchanger on the CORC performance.

The net power output and thermal efficiency of the traditional TORCs are also drawn in Fig. 8 with the dotted lines, which are independent of the PPTD of the internal heat exchanger. As usual, the traditional R245fa-based TORC exhibits the lowest thermodynamic performance. Furthermore, the net power output and thermal efficiency of the CORC are always higher than those of the traditional R123-based TORC when the PPTD of the internal heat exchanger is less than certain threshold value. At the threshold value of the PPTD of the internal heat exchanger, the net power output and thermal efficiency of the CORC have the same values with the traditional R123-based TORC. As shown in Fig. 8, the threshold values of the PPTD of the internal heat exchanger are, respectively, 7.9°C and 1.5°C when the outlet temperatures of the flue gas in the evaporator are 110°C and 130°C. In general, the threshold value of the PPTD of the internal heat exchanger is the function of the inlet temperature T_1 of the flue gas, outlet temperature T_2 of the flue gas, outlet temperature $T_{2'}$ of the flue gas in the evaporator and the inlet pressure P_5 of the expander No.1, as shown in Fig. 9. In general, the CORC can obtain better performance than the traditional TORCs when the PPTD of the internal heat exchanger is less than a certain threshold value.

4.4 Optimal pressure ratio

The above results on thermodynamic performance analysis of the CORC are based on the optimal pressure ratio of the expander. In fact, the optimal pressure ratio depends on the operation conditions of the CORC, as shown in Fig. 10. Note that the maximum pressure ratio of the expander in the CORC is limited to 8.

At T_2 = 90°C, $T_{2'}$ = 120°C, $P_5 = 1.03P_{cri1}$ and ΔT_{ihe} = 5°C, with the increase of the inlet temperature of the flue gas, the optimal pressure ratio ε_{p1} of the expander No.1 decreases first due to the limitation of the PPTD of the evaporator, and then increases, as shown in Fig. 10(a). However, the optimal pressure ratio ε_{p2} of the expander No.2 increases first and then decreases, which varies with the optimal pressure ratio ε_{p1}. At T_1 = 259.5°C, the optimal pressure ratios of the expanders No.1 and 2 have the same values of $\varepsilon_{p1} = \varepsilon_{p2} = 5.52$.

When the inlet and outlet temperatures of the flue gas in the evaporator are fixed, the optimal pressure ratios of the expanders remain constant and are independent of the outlet temperature of the flue gas in the preheater. However, the outlet temperature $T_{2'}$ of the flue gas in the evaporator has an important influence on the optimal pressure ratio, as shown in Fig. 10(b). At T_1 = 270°C, T_2 = 90°C, $P_5 = 1.03P_{cri1}$ and ΔT_{ihe} = 5°C, with the increase of the outlet temperature of the flue gas in the evaporator, the optimal pressure ratio ε_{p1} of the expander No.1 decreases rapidly. At $T_{2'} \geq$ 130°C, it is almost unchanged because of the limitation of the optimal pressure ratio ε_{p2} of the expander No.2. The variation of the optimal

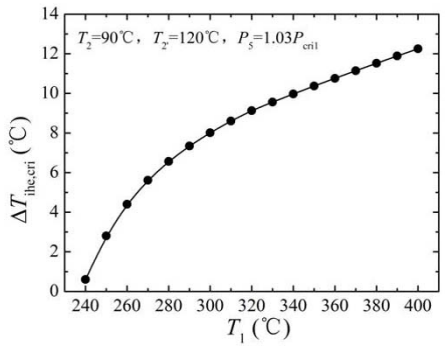

(a)

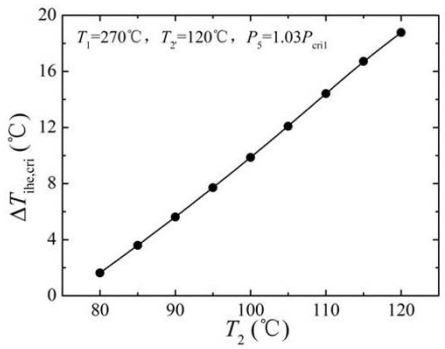

(b)

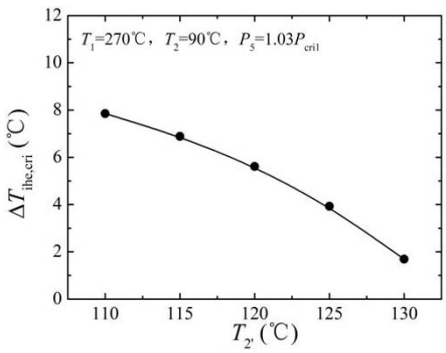

(c)

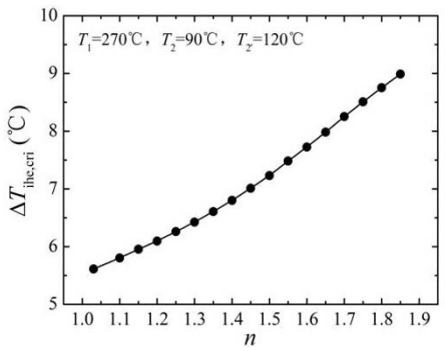

(d)

Fig. 9. Variations of the threshold value of the PPTD of the internal heat exchanger with inlet temperature T_1 of the flue gas (a); outlet temperature T_2 of the flue gas (b); outlet temperature $T_{2'}$ of the flue gas in the evaporator (c); and the inlet pressure P_5 of the expander No.1 (d).

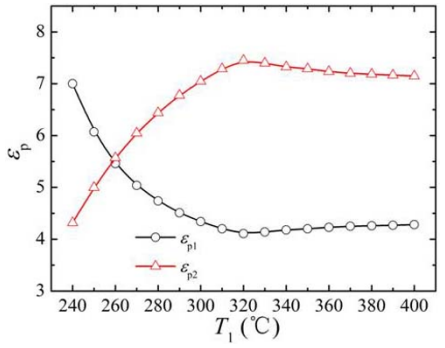

(a)

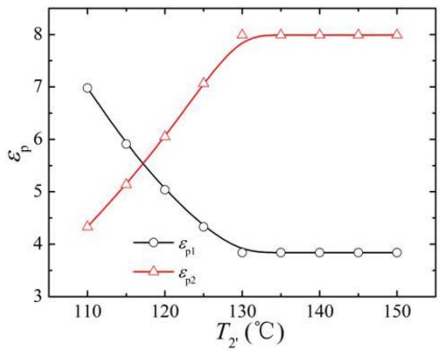

(b)

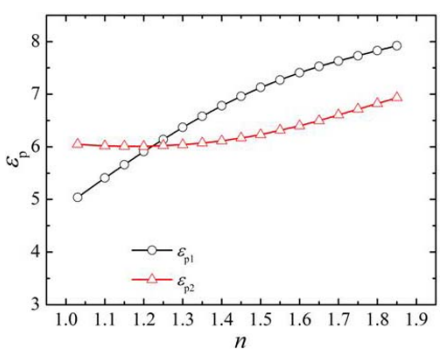

(c)

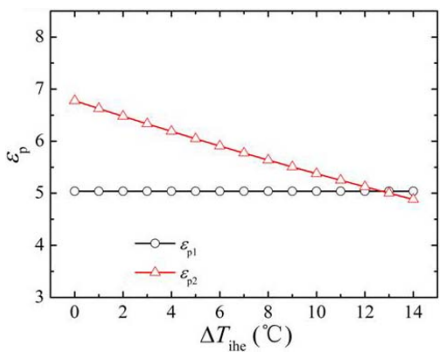

(d)

Fig. 10. Variations of the optimal pressure ratio ε_p with the inlet temperature of the flue gas (a); the outlet temperature of the flue gas in the evaporator (b); the inlet pressure of the expander No.1 (c); and the PPTD of the internal heat exchanger (d).

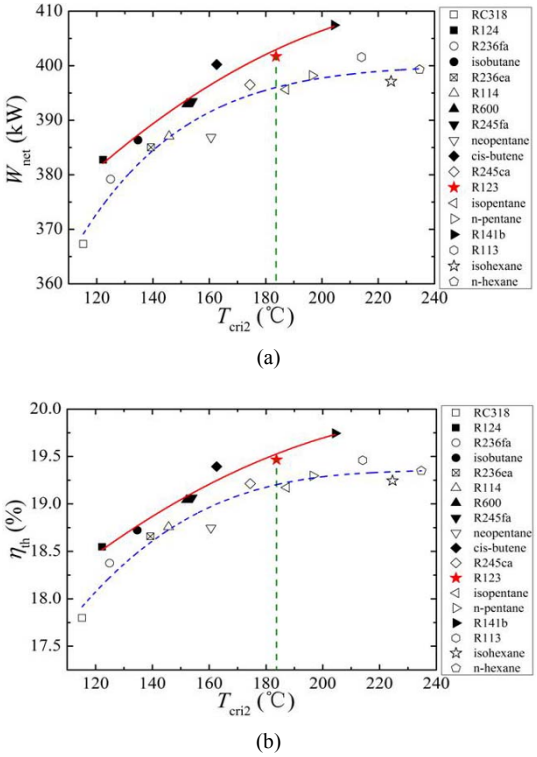

Fig. 11. Variations of net power output W_{net} (a) and thermal efficiency η_{th}; (b) with critical temperature of organic fluids of the SORC at T_1 = 270°C, T_2 = 90°C, $T_{2'}$ = 120°C, P_5 = 1.03P_{cri1} and ΔT_{ihe} = 5°C when R123 is selected as the working fluid of the TORC system. Solid and hollow symbols stand for the isentropic and dry organic working fluid, respectively.

pressure ratio ε_{p2} is opposite. At $T_{2'}$ = 117.2°C, the optimal pressure ratios of the expanders No.1 and 2 have the same values of $\varepsilon_{p1} = \varepsilon_{p2} = 5.54$.

The variation of the pressure ratios with the inlet pressure of the expander No.1 is shown in Fig. 10(c). At T_1 = 270°C, T_2 = 90°C, $T_{2'}$ = 120°C, and ΔT_{ihe} = 5°C, with the increase of the inlet pressure of the expander No.1, the optimal pressure ratio ε_{p1} of the expander No.1 increases, while the optimal pressure ratio ε_{p2} increases after a slight decrease and shows a minimum value. The thermodynamic performance of the TORC subsystem is independent of the PPTD of the internal heat exchanger. Therefore, the optimal pressure ratio ε_{p1} of the expander No.1 remains constant. But the optimal pressure ratio ε_{p2} of the expander No.2 in the SORC subsystem decreases rapidly with the increase of the PPTD of the internal heat exchanger, as shown in Fig. 10(d).

In addition, for the traditional TORCs, the optimal pressure ratio of the expander is much higher than that in the CORC. For example, at P_5 = 1.03P_{cri1} and the same heat source and heat sink conditions, the optimal pressure ratios of the expander in the traditional TORC system with R123 and R245fa as the working fluids are 34.42 and 21.15, respectively. It proves that the CORC system is very efficient in decreasing the optimal pressure ratio of the expander.

5. Effect of the working fluid combinations

The thermodynamic performance of the CORC is related to the physical properties of the organic working fluids. Therefore, it is necessary to select the optimal combination of the working fluids for the CORC. When the heat source and sink conditions are given, the critical temperature T_{cri} of the organic working fluid becomes the key property at the working fluid selection [25]. In this section, eighteen kinds of the organic working fluids are selected and their physical properties are shown in Table 1.

First, R123 is selected as the working fluid of the TORC subsystem and different organic fluids are chosen as the working fluids of the SORC subsystem. Fig. 11 shows the variations of the net power output and thermal efficiency with the critical temperature T_{cri2} of the organic working fluids of the SORC subsystem at T_1 = 270°C, T_2 = 90°C, $T_{2'}$ = 120°C, P_5 = 1.03P_{cri1} and ΔT_{ihe} = 5°C. Solid and hollow symbols stand for the isentropic and dry organic working fluids, respectively. The lines show the variation tendency of the net power output and thermal efficiency with the critical temperature T_{cri2}. It can be found that the net power output of the CORC increases with the increase of the critical temperature T_{cri2} of the organic working fluids of the SORC subsystem. For the isentropic organic fluid, this variation tendency of the net power output is very strict. However, for the dry organic fluid, there are several individual organic fluids that do not satisfy the increase rule, such as neopentane, isopentane and isohexane etc. Furthermore, the net power output with the isentropic organic fluid as the working fluid of the SORC subsystem is always higher than that with the dry organic working fluid. Clearly, the CORC with the working fluid combinations of R123/RC318 and R123/R141b produces the lowest net power output of 367.3 kW and the highest net power output of 407.4 kW, respectively. That the variation of the thermal efficiency of the CORC with the critical temperature T_{cri2} of the organic working fluids of the SORC subsystem is the same with that of the net power output. The lowest and the highest thermal efficiencies are, respectively, 17.80% and 19.74% for the CORC with the working fluid combinations of R123/RC318 and R123/R141b at T_1 = 270°C, T_2 = 90°C, $T_{2'}$ = 120°C, P_5 = 1.03P_{cri1} and ΔT_{ihe} = 5°C.

Second, R245fa is selected as the working fluid of the SORC subsystem, and different organic fluids are chosen as the working fluids of the TORC subsystem. As a result of the limitations of the pressure ratio of the expander and the PPTD of the evaporator, some working fluids with high critical temperature are not suitable for the TORC subsystem, such as R141b, R113, isohexane and n-hexane etc. Fig. 12 shows the variations of the net power output and thermal efficiency with the critical temperature T_{cri1} of the organic working fluids of the TORC subsystem at T_1 = 270°C, T_2 = 90°C, $T_{2'}$ = 120°C, P_5 = 1.03P_{cri1} and ΔT_{ihe} = 5°C. It is found that the net power output of the CORC increases strictly with the increase of the critical temperature T_{cri1} whether the working fluids of the

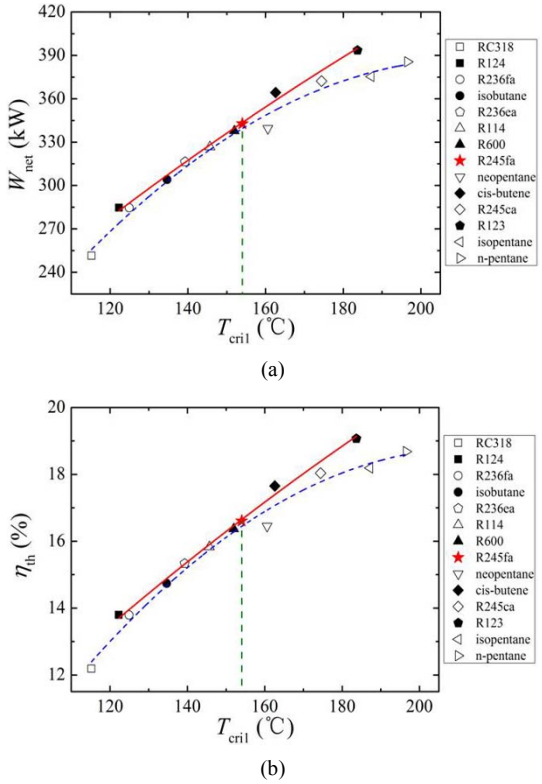

Fig. 12. Variations of net power output W_{net} (a) and thermal efficiency η_{th}; (b) with critical temperature of the working fluid of the TORC subsystem at T_1 = 270°C, T_2 = 90°C, $T_{2'}$ = 120°C, P_5 = 1.03P_{cri1} and ΔT_{ihe} = 5°C when R245fa is selected as the working fluid of the SORC system. Solid and hollow symbols stand for the isentropic and dry organic working fluid, respectively.

TORC subsystem are the dry organic fluid or the isentropic organic fluid. At $T_{cri1} \le T_{cri,\ R245fa}$, the maximum net power output is restricted by the limitation of the pressure ratio of the expander. Therefore, the net power output of the CORC with the isentropic organic working fluid is almost the same as that with the dry organic working fluid. At $T_{cri1} > T_{cri,\ R245fa}$, the net power output of the CORC with the isentropic organic working fluid is higher than that with the dry organic working fluid, as shown in Fig. 12(a). In this case, the CORCs with the working fluid combinations of RC318/R245fa and R123/R245fa produce the lowest net power output of 251.5 kW and the highest net power output of 393.5 kW, respectively. Accordingly, the variation of the thermal efficiency with the critical temperature T_{cri1} is also the same as that of the net power output. The lowest and the highest thermal efficiencies are, respectively, 12.19% and 19.07% for the CORC with the working fluid combinations of RC318/R245fa and R123/R245fa at T_1 = 270°C, T_2 = 90°C, $T_{2'}$ = 120°C, P_5 = 1.03P_{cri1} and ΔT_{ihe} = 5°C.

The different working fluid combinations result in different thermodynamic performance of the CORC. At T_1 = 270°C, T_2 = 90°C, $T_{2'}$ = 120°C and P_5 = 1.03P_{cri1}, the typical results of the CORC with different working fluid combinations are listed in Table 4. The thermodynamic performance of the CORC is better than that of the traditional TORCs. Especially, the net power output and thermal efficiency of the CORC at ΔT_{ihe} = 0°C are much higher than those of the traditional TORCs. As stated earlier, the limitation of the pressure ratio of the expander in the traditional TORC is neglected. Therefore, the pressure ratio in the traditional TORC system is higher than that in the CORC, where the maximum pressure ratio in the CORC is 8. From Table 4, the CORC with R123/R141b yields the best performance with the net power output of 407.4 kW and the thermal efficiency of 19.7%.

Table 4. The typical results with different working fluid combinations at T_1 = 270°C, T_2 = 90°C, $T_{2'}$ = 120°C and P_5 = 1.03P_{cri1}.

Cycle	Working fluids	ΔT_{ihe} °C	η_{th} %	W_{net} kW	ε_{p1}	ε_{p2}
CORC	R236ea/R124	0	15.13	312.3	2.71	4.58
	R236ea/R124	5	14.68	303.0	2.42	4.60
TORC	R236ea	-	13.89	286.7	14.76	-
	R124	-	13.33	275.0	8.38	-
CORC	R600/isobutane	0	16.38	388.1	2.75	4.59
	R600/isobutane	5	15.93	328.7	2.48	4.61
TORC	R600	-	15.56	321.1	13.8	-
	Isobutane	-	13.72	283.2	9.24	-
CORC	Neopentane/R114	0	16.45	339.4	2.45	6.81
	Neopentane/R114	5	16.05	331.1	2.45	6.18
TORC	Neopentane	-	14.45	298.3	16.41	-
	R114	-	14.59	301.2	13.36	-
CORC	R123/R245fa	0	19.56	403.6	5.04	6.78
	R123/R245fa	5	19.07	393.5	5.04	6.05
TORC	R123	-	19.00	392.2	34.42	-
	R245fa	-	15.86	327.4	21.15	-
CORC	R123/R141b	0	20.33	419.47	5.04	6.85
	R123/R141b	5	19.74	407.44	5.04	6.10
TORC	R123	-	19.00	392.2	34.42	-
	R141b	-	21.07	434.78	46.03	-
CORC	Isopentane/cis-butene	0	19.06	393.3	5.05	5.42
	Isopentane/cis-butene	5	18.52	382.2	5.05	4.90
TORC	Isopentane	-	17.09	352.8	31.87	-
	Cis-butene	-	17.89	369.2	17.39	-
CORC	n-pentane/R245ca	0	19.36	399.6	7.16	6.21
	n-pentane/R245ca	5	18.81	388.1	7.16	5.49
TORC	n-pentane	-	18.01	371.6	42.33	-
	R245ca	-	17.23	355.6	33.23	-

6. Conclusions

A novel coupled system driven by waste heat is proposed that combines the transcritical organic Rankine cycle with the subcritical organic Rankine cycle. A detailed perform-

ance analysis on the novel CORC system is performed with the net power output and thermal efficiency as the performance indicators. The following conclusions can be summarized:

(1) The CORC system can decrease the pressure ratio, and the section of the working fluids becomes more flexible and abundant. Within the calculation range, the net power output and thermal efficiency of the CORC are increased with the increase of the inlet temperature and the decrease of the outlet temperature of the flue gas.

(2) With the increase of the PPTD of the internal heat exchanger, the net power output and thermal efficiency of the CORC decrease. When the PPTD of the internal heat exchanger is less than certain threshold value, the net power output and thermal efficiency of the CORC are always higher than those of the traditional TORC with the same working fluids. This threshold value depends on the inlet and outlet temperatures of the flue gas, and the inlet pressure of the expander.

(3) With the increase of the inlet pressure of the expander, the net power output and thermal efficiency of the CORC increase. However, the optimal pressure ratio of the expander corresponding to the maximum net power output is determined by the inlet temperature and the outlet temperature of the flue gas, the inlet pressure of the expander, the PPTD of the internal heat exchanger, and the limitations of the pressure ratio and the PPTD of the evaporator.

(4) With the increase of the critical temperature of the working fluid, the performance of the CORC is improved. The net power output and thermal efficiency of the CORC with isentropic working fluids are always higher than those with dry working fluids. At the given conditions, the CORC with R123/R141b as the working fluids yields the highest net power output and thermal efficiency as 407.4 kW and 19.74%, respectively.

Acknowledgment

This work is supported by National Basic Research Program of China (973 Program, Grant No. 2011CB710701) and National Natural Science Foundation of China (Grant No. 51179174).

Nomenclature

c_p : Specific heat capacity, kJ/(kg·K)
h : Specific enthalpy, kJ/kg
m : Mass flow rate, kg/s
M : Molecular weight, kg/kmol
ρ : Density, kg/m^3
P : Pressure, Pa
Q : Heat transfer rate, W
s : Specific entropy, kJ/(kg·K)
T : Temperature, °C
W : Power output, W

Greek symbols

ε_p : Pressure ratio
η : Efficiency

Subscripts

c : Condenser
cri : Critical value
e : Evaporator
exp : Expander
g : Flue gas
ihe : Internal heat exchanger
net : Net power output
p : Pump
pre : Preheater
t : Total
th : Thermal
w : Water
wf : Working fluid

Acronyms

CORC : Coupled organic Rankine cycle
ORC : Organic Rankine cycle
PPTD : Pinch point temperature difference
SORC : Subcritical organic Rankine cycle
TORC : Transcritical organic Rankine cycle

References

[1] D. H. Wei, X. S. Lu, Z. Lu and J. M. Gu, Performance analysis and optimization of organic Rankine cycle (ORC) for waste heat recovery, *Energy Conversion and Management*, 48 (4) (2007) 1113-1119.

[2] H. J. Chen, D. Y. Goswami and E. K. Stefanakos, A review of thermodynamic cycles and working fluids for the conversion of low-grade heat, *Renewable and Sustainable Energy Reviews*, 14 (2010) 3059-3067.

[3] J. Guo, M. Xu and L. Cheng, Thermodynamic analysis of waste heat power generation system, *Energy*, 35 (7) (2010) 2824-2835.

[4] D. Wang, X. Ling, H. Peng, L. Liu and L. Tao, Efficiency and optimal performance evaluation of organic Rankine cycle for low grade waste heat power generation, *Energy*, 50 (2013) 343-352.

[5] Z. Q. Wang, N. J. Zhou, J. Guo and X. Y. Wang, Fluid selection and parametric optimization of organic Rankine cycle using low temperature waste heat, *Energy*, 40 (1) (2012) 107-115.

[6] S. Quoilin, S. Declaye, B. F. Tchanche and V. Lemort, Thermo-economic optimization of waste heat recovery organic Rankine cycles, *Applied Thermal Engineering*, 31 (14) (2011) 2885-2893.

[7] Q. C. Chen, J. L. Xu and H. X. Chen, A new design

method for organic Rankine cycles with constraint of inlet and outlet heat carrier fluid temperatures coupling with the heat source, *Applied Energy*, 98 (2012) 562-573.

[8] A. Borsukiewicz-Gozdur, Exergy analysis for maximizing power of organic Rankine cycle power plant driven by open type energy source, *Energy*, 62 (2013) 73-81.

[9] S. L. Milora and J. W. Tester, Geothermal energy as a source of electric power: Thermodynamic and economic design criteria, *NASA STI/Recon Technical Report A*, 77 (1976) 16623.

[10] G. L. Mines, *Test plan for heat cycle research program, Phase I Supercritical Cycle Tests*, USDOE Office of Energy Efficiency and Renewable Energy Geothermal Technology Program (1983).

[11] K. Gawlik and V. Hassani, Advanced binary cycles: Optimum working fluids, *Proceedings of the 32nd Intersociety of Energy Conversion Engineering Conference*, 3 (1997) 1809-1814.

[12] A. Algieri and P. Morrone, Comparative energetic analysis of high-temperature subcritical and transcritical organic Rankine cycle (ORC), A biomass application in the Sibari district, *Applied Thermal Engineering*, 36 (2012) 236-244.

[13] S. J. Zhang, H. X. Wang and T. Guo, Performance comparison and parametric optimization of subcritical organic Rankine cycle (ORC) and transcritical power cycle system for low-temperature geothermal power generation, *Applied Energy*, 88 (8) (2011) 2740-2754.

[14] D. Mikielewicz and J. Mikielewicz, A thermodynamic criterion for selection of working fluid for subcritical and supercritical domestic micro CHP, *Applied Thermal Engineering*, 30 (16) (2010) 2357-2362.

[15] N. A. Lai, M. Wendland and J. Fischer, Working fluids for high-temperature organic Rankine cycles, *Energy*, 36 (1) (2011) 199-211.

[16] G. Q. Qiu, H. Liu and S. Riffat, Expanders for micro-CHP systems with organic Rankine cycle, *Applied Thermal Engineering*, 31 (16) (2011) 3301-3307.

[17] J. Bao and L. Zhao, A review of working fluid and expander selections for organic Rankine cycle, *Renewable and Sustainable Energy Reviews*, 24 (2013) 325-342.

[18] H. G. Zhang, H. Liang, X. Liu, B. Liu, Y. Chen, Y. T. Wu, W. Wang and K. Yang, Research of two stage single screw expander organic Rankine cycle system scheme based on the waste heat recovery of diesel engine's exhaust gas, *Advanced Materials Research*, 201 (2011) 600-6005.

[19] D. W. Hanner, J. L. McElroy, E. Robinson and W. M. Wells, High-temperature testing and evaluation of graphite helical-screw expanders and compressors, *J. of Spacecraft and Rockets*, 4 (6) (1967) 761-767.

[20] D. W. Taitt, C. P. Garner, E. Swain, D. Blundell, R. J. Pearson and J. W. G. Turner, An automotive engine charge-air intake conditioner system: analysis of fuel economy benefits in a gasoline engine application, *Proceedings of the Institution of Mechanical Engineers, Part D: J. of Automobile Engineering*, 220 (9) (2006) 1293-1307.

[21] E. H. Wang, H. G. Zhang, B. Y. Fan, M. G. Ouyang, Y. Zhao and Q. H. Mu, Study of working fluid selection of organic Rankine cycle (ORC) for engine waste heat recovery, *Energy*, 36 (5) (2011) 3406-3418.

[22] H. G. Zhang, E. H. Wang, M. G. Ouyang and B. Y. Fan, Study of parameters optimization of organic Rankine cycle (ORC) for engine waste heat recovery, *Advanced Materials Research*, 201 (2011) 585-589.

[23] E. H. Wang, H. G. Zhang, Y. Zhao, B. Y. Fan, Y. T. Wu and Q. H. Mu, Performance analysis of a novel system combining a dual loop organic Rankine cycle (ORC) with a gasoline engine, *Energy*, 43 (1) (2012) 385-395.

[24] D. Meinel, C. Wieland and H. Spliethoff, Effect and comparison of different working fluids on a two-stage organic rankine cycle (ORC) concept, *Applied Thermal Engineering*, 63 (1) (2014) 246-253.

[25] J. L. Xu and C. Liu, Effect of the critical temperature of organic fluids on supercritical pressure organic Rankine cycles, *Energy*, 63 (2013) 109-122.

[26] *REFPROP Version 8.0*, NIST standard reference database 23 (2007).

[27] J. M. Calm and G. C. Hourahan, Refrigerant data update, *HPAC Engineering*, 1 (2007) 50-64.

[28] E. Cayer, N. Galanis and H. Nesreddine, Parametric study and optimization of a transcritical power cycle using a low temperature source, *Applied Energy*, 87 (4) (2010) 1349-1357.

[29] Y. H. Song, J. F. Wang, Y. P. Dai and E. M. Zhou, Thermodynamic analysis of a transcritical CO_2 power cycle driven by solar energy with liquified natural gas as its heat sink, *Applied Energy*, 92 (2012) 194-203.

[30] T. Guo, H. X. Wang and S. J. Zhang, Comparative analysis of CO_2-based transcritical Rankine cycle and HFC245fa-based subcritical organic Rankine cycle using low-tempera-ture geothermal source, *Science China Technological Sciences*, 53 (6) (2010) 1638-1646.

[31] F. Vélez, J. Segovia, F. Chejne, G. Antolin, A. Quijano and M. C. Martin, Low temperature heat source for power generation: Exhaustive analysis of a carbon dioxide transcritical power cycle, *Energy*, 36 (9) (2011) 5497-507.

[32] T. Guo, H. X. Wang and S. J. Zhang, Comparative analysis of natural and conventional working fluids for use in transcritical Rankine cycle using low-temperature geothermal source, *International J. of Energy Research*, 35 (6) (2011) 530-544.

[33] Y. J. Baik, M. Kim, K. C. Chang and S. J. Kim, Power-based performance comparison between carbon dioxide and R125 transcritical cycles for a low-grade heat source, *Applied Energy*, 88 (3) (2011) 892-898.

[34] Y. Chen, P. Lundqvist, A. Johansson and P. Platell, A comparative study of the carbon dioxide transcritical power cycle compared with an organic Rankine cycle with R123 as working fluid in waste heat recovery, *Applied Thermal Engineering*, 26 (17) (2006) 2142-2147.

[35] Z. Gu and H. Sato, Performance of supercritical cycles for geothermal binary design, *Energy Conversion and Management*, 43 (7) (2002) 961-971.

[36] K. C. Ng, T. B. Lim and T. Y. Bong, Analysis of screw-expander performance, *Proceedings of the Institution of mechanical engineers, Part E: J. of Process Mechanical Engineering*, 203 (1) (1989) 15-20.

[37] S. Clemente, D. Micheli, M. Reini and R. Taccani, Performance analysis and modeling of different volumetric expanders for small-scale organic Rankine cycles, *ASME 2011 5th International Conference on Energy Sustainability*, American Society of Mechanical Engineers (2011) 375-384.

[38] S. Declaye, S. Quoilin, L. Guillaume and V. Lemort, Experimental study on an open-drive scroll expander integrated into an ORC (organic Rankine cycle) system with R245fa as working fluid, *Energy*, 55 (2013) 173-183.

[39] A. Schuster, S. Karellas and R. Aumann, Efficiency optimization potential in supercritical organic Rankine cycles, *Energy*, 35 (2) (2010) 1033-1039.

Xi-Wu Gong received his M.S. from Anhui University of Science & Technology, Huainan, China, in 1996, obtained his Ph.D. in Engineering Thermophysics from Shanghai Jiaotong University in 2008. He is an associate professor at Zhejiang Ocean University. His major interests are heat transfer, thermodynamics, energy conversion and saving.

You-Rong Li received his Ph.D. from the College of Power Engineering, Chongqing University, Chongqing, China, in 1999, and worked as a Postdoctoral Fellow in Institute of Advanced Material Study, Kyushu University, Japan, during 2000-2002. He is a professor at Chongqing University. His major interests are engineering thermodynamics, convective heat transfer, thermocapillary flow and stability.